engineering proceedings

MDPI

Proceeding Paper

On the Design of a GaN-Based Solid-State Circuit Breaker for On-Board DC Microgrids †

Symeon Fountoukidis [1], Nick Rigogiannis [1], Georgios Voltsis [1], Konstantinos Terzopoulos [2], Michael Loupis [2] and Nikolaos Papanikolaou [1,*]

[1] Department of Electrical and Computer Engineering, Democritus University of Thrace, 67100 Xanthi, Greece; sfountou@ee.duth.gr (S.F.); nrigogia@ee.duth.gr (N.R.); georvolt@ee.duth.gr (G.V.)
[2] General Department, National and Kapodistrian University, 15772 Athens, Greece; kterzo@uoa.gr (K.T.); mloupis@uoa.gr (M.L.)
* Correspondence: npapanik@ee.duth.gr
† Presented at the 4th International Conference on Communications, Information, Electronic and Energy Systems (CIEES 2023), Plovdiv, Bulgaria, 23–25 November 2023.

Abstract: The concept of more electric aircraft (MEA) has gained popularity over the last few decades. As the power level of electric loads is constantly increasing, the installation of advanced protection systems becomes of paramount importance. In this context, this paper presents the design process and experimental validation of a solid-state circuit breaker (SSCB), utilizing gallium nitride (GaN) semiconductor switches, under various faulty conditions. In addition, a thermal analysis was carried out in the PLECS simulation platform to find the most appropriate design for the heat dissipation system. Experimental results on the developed GaN SSCB hardware prototype verify its functionality and good performance.

Keywords: DC microgrids; gallium nitride (GaN); more electric aircraft (MEA); solid-state circuit breaker (SSCB)

Citation: Fountoukidis, S.; Rigogiannis, N.; Voltsis, G.; Terzopoulos, K.; Loupis, M.; Papanikolaou, N. On the Design of a GaN-Based Solid-State Circuit Breaker for On-Board DC Microgrids. *Eng. Proc.* **2024**, *60*, 16. https://doi.org/10.3390/engproc2024060016

Academic Editor: Renato Filjar

Published: 10 January 2024

1. Introduction

The more electric aircraft (MEA) concept has emerged over the last few decades as a promising solution for greener transportation with enhanced performance, reduced greenhouse gas emissions, and less dependence on carbon-based fossil fuels [1]. MEA distribution networks are constantly evolving, moving from purely AC to hybrid configurations, whereas purely DC microgrid architectures have been proposed for future aircraft [2]. In parallel, these power electronic-dominated grids comprise various power sources with particular characteristics, hybrid energy storage systems, and tightly controlled electronic loads with specific power demands (e.g., constant power, pulsed power, intermittent operation, etc.) [3].

In this light, new challenges arise regarding the protection of on-board DC distribution networks. Traditionally, MEA protection systems were based on conventional circuit breakers (CBs), which include magnetothermal elements [4], breaking the circuit before the current reaches its peak value or when the maximum tripping time has passed. Nevertheless, CBs are not able to detect arc faults, as they have a very short duration. Thus, CBs are considered inappropriate for such applications. Another more recently introduced option is the arc-fault circuit breaker (AFCB), which features the same operating principle as CBs, yet it is capable of protecting the DC microgrid against electric arc faults [5].

Moreover, the remote control and monitoring of the electric power distribution system's characteristics (i.e., current and voltage setpoints) are of paramount importance; however, this feature is not supported by AFCBs. A device incorporating the functionality of CBs allowing for remote management is the remote control circuit breaker (RCCB).

However, its slow response time (i.e., from 15 ms to several seconds) may jeopardize the overall system operation; thus, RCCBs are considered unsuitable for MEA applications [5].

With the notable advancements in semiconductor material technology during the last few decades, SSCBs have gained popularity for such installations because of their ability to provide rapid circuit breaking in cases of faults. Furthermore, with the inverse time control loop (I^2t), SSCBs feature overheating protection while being capable of effectively handling fault interruptions under normal transient conditions (e.g., inrush currents) [6]. Their additional features include high reliability, efficiency, and power density.

In parallel, in order to exceed the performance limits of typical Si semiconductor switches that have been extensively used in a wide range of power electronic applications, new wide-bandgap (WBG) materials have been developed for such applications [7]. SiC and GaN are the most popular WBG materials used in power switches. Specifically, GaN-based FETs have been reported in recent scientific research as an appropriate option for SSCB implementation, because of their improved performance in terms of efficiency (i.e., low conduction losses due to the low turn-on resistance values, $R_{ds,on}$) and thermal conductivity, which leads to lower heatsink size [7,8]. Additionally, the enhanced electron mobility and saturation velocity of GaN are related to improved switching characteristics, leading to considerably decreased turn-off times [7]. As for the GaN transistor market, currently, devices in the 600 V and 650 V classes are commercially available.

Various recently published papers investigate the behavior of SSCBs in both short circuits and steady-state operation (e.g., in [9]). Regarding the GaN-based SSCBs, in [10], an extensive study on the robustness of 650 V GaN HEMTs under short-circuit conditions, for various gate drive voltages and temperatures was performed. Moreover, this study revealed the device degradation trends after repetitive fault tests. In parallel, Ref. [11] focused on distribution networks' protection by SSCBs by adopting parallel GaN bidirectional switches. Minimum conduction losses, as well as high current fault clearing in the μs scale, were obtained (i.e., interruption of 306 A in 1.2 μs). Furthermore, in [12], the design of a GaN-based switch rated at 45 A for both 380 V DC and 230 V AC grids is presented, along with its thermal analysis, to provide the temperature rise for various operating conditions.

In this context, this work involves a study of the implementation of a GaN-based SSCB for the protection of low-voltage DC microgrids, applicable to MEA. A complete thermal design is also provided, and the I^2t current-limiting control strategy is digitally implemented. Experimental results in a 48 V laboratory-scale DC microgrid are obtained, validating the functionality of the proposed design. The rest of this paper is organized as follows: In Section 2, the proposed system (both power and control stages) is presented and analyzed in detail. Next, in Section 3, the studied system is modeled and simulated in PLECS, and more details on the developed hardware prototype, as well as experimental results, are presented. Finally, Section 4 concludes the paper.

2. System Description

2.1. System Overview

Significant effort has been made by researchers and engineers to find the most appropriate topologies for SSCB applications [13]. Thanks to its minimized power losses and few component count, this topology is considered the most suitable for high-power applications, specifically for MEA. The operating states for steady-state and short-circuit cases are depicted in Figure 1. State 1 corresponds to the steady-state condition, in which MOSFET switches are turned on, and the current reaches its nominal value; thus, in this state, the conductive path is provided for the fault current before the tripping time (predefined turn-off delay) is exceeded.

After this point, MOSFETs transition to State 2; the energy is stored in a feeder inductance (L_{cable}) and charges the snubber capacitor with the help of a freewheeling MOSFET body diode. When the body diode is turned off, the fault current decreases, transitioning so to State 3. The stored charge in the capacitor starts discharging through the snubber resistances during this state. This configuration can accommodate the bidirectional current flow.

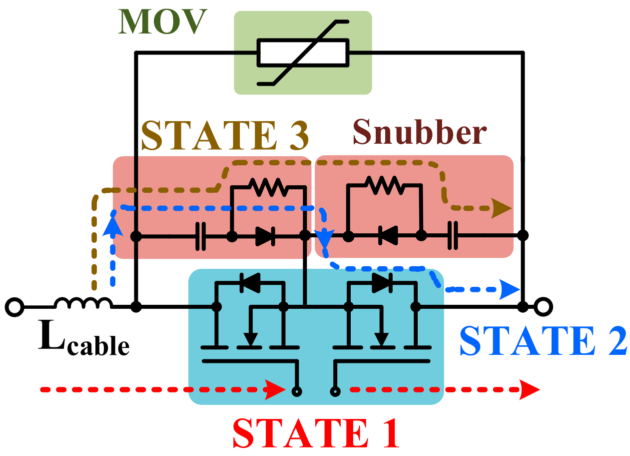

Figure 1. Operating states of the common source SSCB topology.

The clearing of the maximum fault current (e.g., solid short circuit), as well as the sudden disconnection of the fault side, leads to overvoltages across the SSCB device, which may result in much higher voltage levels than the nominal value. These overvoltages are caused by the feeder inductor's stored energy. A solution to this issue is the addition of a snubber circuit, as mentioned above. When the feeder's stored energy exceeds the snubber's handling capability, additional measures can be taken, such as the use of transient voltage suppressors (TVSs). Ideally, in steady state mode, no current flows through the TVS; yet, during fault conditions, it acts as a short circuit, preventing damage due to overvoltages. Aside from TVSs, metal oxide varistors (MOVs) can be used for high-energy dissipation. MOVs operate as resistors and offer higher surge voltages and current ratings than TVS devices [14].

2.2. Detailed Description of the I^2t Control Strategy

Regarding the controller implementation, the SSCB operates under the inverse time protection scheme (I^2t), where different fault current values correspond to a different (predefined) tripping time delay, avoiding unnecessary interruptions in cases of temporary faults. Figure 2 illustrates the considered I^2t curve, in which two areas can be distinguished; area 1 represents a solid short circuit (i.e., the maximum fault current, which can reach ten times the nominal steady-state value), and area 2 represents the I^2t response, in which the current varies from low values to approximately nine times the nominal one, and the tripping time varies accordingly. It should be noted that a solid short circuit can be instantly interrupted (i.e., the upper limit of 3 ms is determined by considering the maximum delay due to the driving circuit and the control loop's digital implementation).

The aforementioned I^2t control strategy is digitally implemented with the aid of the TMS320F8379D microcontroller provided by Texas Instruments, using the PLECS coder. Such a microcontroller is a convenient solution for digital control in power electronic applications, as it incorporates analog comparators with ramp generators, error amplifiers, and several PWM and ADC modules in a single IC, minimizing the need for additional external components [15].

The main modules for the digital implementation of the current control scheme are the ePWM and the ADC. Various blocks from the PLECS library (e.g., timers) are used to implement the control algorithm. Furthermore, the external mode operation allows for the real-time monitoring of the measured signals of the standalone model. Finally, with code generation via PLECS, the programming effort is minimized. Figure 3 presents the block diagram of the control scheme implemented in PLECS (version 4.7.5) simulation software.

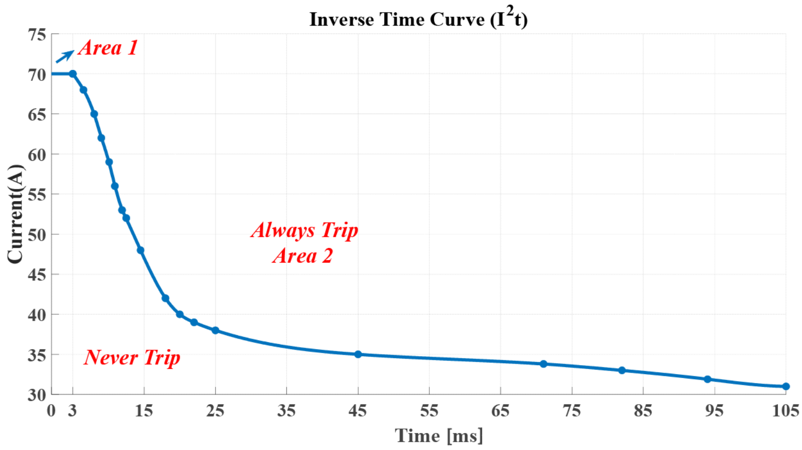

Figure 2. The current limiting control strategy, based on the I^2t curve.

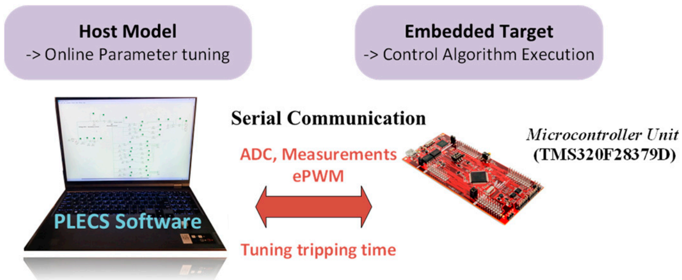

Figure 3. Block diagram of the control system.

3. Simulation and Experimental Results

3.1. Thermal Analysis of the SSCB

During fault conditions (e.g., short circuits), a high increase in junction temperature ($T_{junction}$) is expected, due to excessive heat dissipation. In steady-state operation, $T_{junction}$ can be estimated by using Expression (1). In this operating mode, the temperature rise is not significant when the I^2t control is activated, although increased current levels beyond the nominal value (e.g., due to repetitive faults) may accelerate the aging of the semiconductor device. Consequently, the selection of power devices with suitable thermal characteristics is of paramount importance, in order to operate the device within the safe operation area (SOA), during both steady-state and transient conditions.

Additionally, the SSCB thermal model can be obtained by the thermal impedance from junction to ambient ($Z_{th,ja}$), which is calculated from the sum of the intermediate thermal impedances (i.e., $Z_{th,ja} = Z_{th,jc} + R_{th,cs} + R_{th,ca}$). The junction-to-case thermal impedance ($Z_{th,jc}$) is determined by the GaN semiconductor's characteristics. Moreover, the case-to-ambient thermal resistance ($R_{th,ca}$) is related to the size, shape, and material of the heatsink. Thus, the proper selection of the cooling means is imperative to maintain the temperature rise within the SOA and optimize the overall system power density.

$$P_{max} = \frac{T_{junction} - T_{ambient}}{R_{th,ja}} \tag{1}$$

The main characteristics of the studied system are presented in Table 1. The full-scale SSCB configuration comprised three parallel branches (i.e., three common-source switches connected in parallel), and it was connected to a 48 V DC bus, considering the maximum (worst case scenario, i.e., a solid short circuit) current at 70 A. Two GaN HEMT thermal models were imported into the PLECS software for the 100 V class. Specifically, the GS1008 and GS6516 devices, provided by GaN Systems, were selected, and they complied with the studied system specifications. Simulation results are presented in Figure 4. It is worth noting that the simulation tests were carried out considering a solid short circuit of 120 A, which is the maximum allowable (pulsed) current for the specific GaN transistors. GS6516 was found to be unsuitable for the specific application, as its operation within the SOA limits was satisfied only for extremely low thermal resistances, leading to an increase in the cooling system volume and thus reduced power density.

Table 1. Main parameters of the full-scale studied system.

Component/Symbol	Actual Value (Description)
	GaN HEMT GS1008 (GaN Systems)
R_{DS_ON}	7 mΩ (FET on resistance)
V_{DS}	100 V (breakdown voltage)
T_{jmax}	150 °C (maximum temperature in steady-state operation)
L_{cable}	10 µH *
R_{cable}	1 mΩ *
	Snubber
$C_{snubber}$	16 µF (snubber capacitance)
$R_{snubber}$	7.5 Ω (snubber resistance, rated at 10 W)
V_{DC}	48 V (bus voltage)

* Equivalent series feeder inductance.

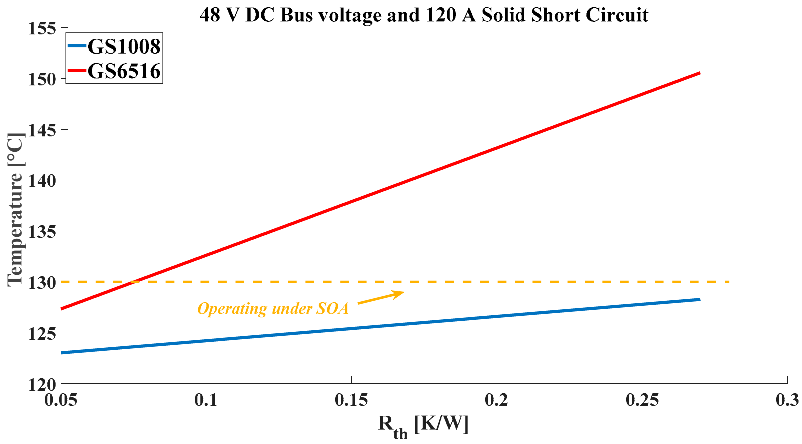

Figure 4. Simulation results for the 48 V DC bus and 120 A solid short-circuit test, for various thermal resistances.

Furthermore, Figure 5 illustrates the thermal behavior of the GS1008 transistor under the operation of the I^2t current limiting strategy presented in Figure 2. The increase in the fault current value barely influenced the temperature rise, whereas different thermal resistance values led to different temperature values. Therefore, finding the desired operating temperature during fault conditions led to the selection of suitable thermal resistance. In order not to accelerate device aging, the appropriate temperature was selected to be below 100 °C; therefore, the 10 K/W thermal resistance value was selected to maintain the volume and weight of the cooling system at acceptably low levels.

3.2. Experimental Validation

The previously discussed thermal analysis revealed the optimal thermal resistance value for operation within the limits of SOA, as well as the most appropriate GaN HEMT of the two options. This subsection focuses on the experimental investigation of the designed GaN-based SSCB prototype. A scaled-down configuration comprising only one of the three parallel branches was developed; a solid short-circuit current of 20 A was considered, and the feeder inductance was 127 µH to obtain the same thermal characteristics as the full-scale simulated system; the rest of its features were the same as those presented in

Table 1. Figure 6 shows the response of the developed protection device during an instant solid short circuit (trip fault). The total delay time did not exceed 1.5 ms. Therefore, the superior circuit-breaking performance of the GaN-based SSCB is highlighted, compared to conventional mechanical CBs.

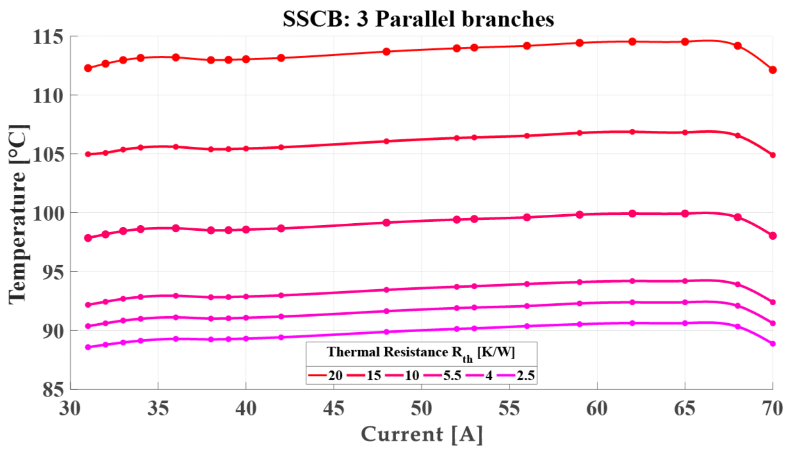

Figure 5. Estimation of the temperature rise during fault conditions (I^2t protection scheme is considered) with the aid of PLECS software.

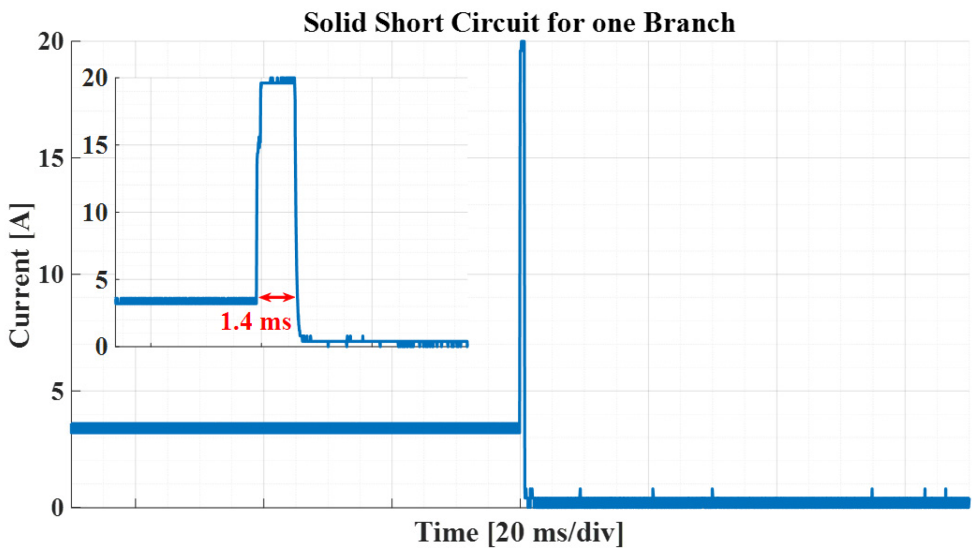

Figure 6. Experimental results for the solid short-circuit test.

Last but not least, an experimental test with multiple faults/overloading conditions was performed to examine various current levels of the I^2t curve; experimental results are presented in Figure 7. In these tests, overvoltages were detected, caused by the excessive energy that dissipated at the SSCB. Thanks to the proper design of the snubber circuit, voltage spikes did not exceed the GaN transistor breakdown voltage in any of the fault cases.

In parallel, the results of the experimental procedure reveal that the digital implementation of the I^2t protection scheme facilitates extremely low response times to faults, with minimized delays. This enhances the reliability and robustness of the low-voltage DC microgrid, which is essential in MEA applications. Overall, the proper design of the GaN-based SSCB, from both an electrical and thermal point of view, ensures the secure, reliable, and uninterruptible operation of the DC network.

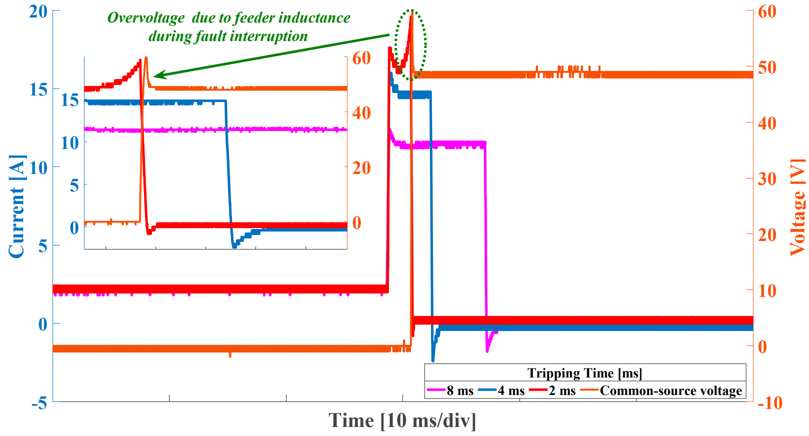

Figure 7. Experimental results for various fault cases (I^2t protection scheme was considered).

4. Conclusions

In this work, the design and development of a GaN-based SSCB with a digitally implemented I^2t protection scheme were presented as a promising protection device for MEA low-voltage DC microgrids. The proper thermal analysis and design were discussed to obtain highly efficient operation with minimum size and weight of the cooling system. Experimental results indicate the functionality and good performance of the designed SSCB in a wide range of faults, with fast response, highlighting its superiority over conventional CBs.

Author Contributions: Conceptualization, S.F., N.R., M.L. and N.P.; methodology, S.F., N.R., G.V. and K.T.; software, S.F. and G.V.; validation, S.F., N.R., G.V. and K.T.; formal analysis, S.F., N.R. and G.V.; investigation, S.F., N.R., G.V. and K.T.; resources, S.F., G.V. and K.T.; data curation, S.F., N.R. and G.V.; writing—original draft preparation, S.F., N.R. and G.V.; writing—review and editing, S.F., N.R., M.L. and N.P.; visualization, S.F. and G.V.; supervision, M.L. and N.P.; project administration, N.P. All authors have read and agreed to the published version of the manuscript.

Funding: This research was co-financed by the European Regional Development Fund of the European Union and Greek national funds through the Operational Program for Competitiveness, Entrepreneurship and Innovation, under the call RESEARCH–CREATE–INNOVATE (project code: T2EDK-00136).

Institutional Review Board Statement: Not applicable.

Informed Consent Statement: Not applicable.

Data Availability Statement: No new data were created or analyzed in this study. Data sharing is not applicable to this article.

Conflicts of Interest: The authors declare no conflicts of interest.

References

1. Sarlioglu, B.; Morris, C.T. More Electric Aircraft: Review, Challenges, and Opportunities for Commercial Transport Aircraft. *IEEE Trans. Transp. Electrif.* **2015**, *1*, 54–64. [CrossRef]
2. Rigogiannis, N.; Voglitsis, D.; Jappe, T.; Papanikolaou, N. Voltage Transients Mitigation in the DC Distribution Network of More/All Electric Aircrafts. *Energies* **2020**, *13*, 4123. [CrossRef]
3. Rigogiannis, N.; Papanikolaou, N.; Yang, Y. Performance Enhancement of Power Conditioning Systems in More Electric Aircrafts. In Proceedings of the 2022 24th European Conference on Power Electronics and Applications (EPE'22 ECCE Europe), Hanover, Germany, 5–9 September 2022; pp. 1–9.
4. Bozhko, S.; Hill, C.I.; Yang, T. More-Electric Aircraft: Systems and Modeling. In *Wiley Encyclopedia of Electrical and Electronics Engineering*; John Wiley & Sons, Inc.: Hoboken, NJ, USA, 2018; pp. 1–31. [CrossRef]
5. Izquierdo, D.; Barrado, A.; Sanz, M.; Lázaro, A.; Barrado, A.; Raga, C. Protection Devices for Aircraft Electrical Power Distribution Systems: State of the Art. *IEEE Trans. Aerosp. Electron. Syst.* **2011**, *47*, 1538–1550. [CrossRef]

6. Fountoukidis, S.; Rigogiannis, N.; Papanikolaou, N.; Loupis, M. Digital Implementation of I2t Protection Scheme by means of Solid-State Devices. In Proceedings of the 2023 12th International Conference on Modern Circuits and Systems Technologies (MOCAST), Athens, Greece, 28–30 June 2023; pp. 1–5. [CrossRef]
7. Rigogiannis, N.; Kotsidimou, A.; Arzanas, I.; Kyritsi, C.; Papanikolaou, N. Comparative Performance Study of Hybrid Si/SiC Insulated-Gate Bipolar Transistors. In Proceedings of the 2022 IEEE 7th Forum on Research and Technologies for Society and Industry Innovation (RTSI), Paris, France, 24–26 August 2022; pp. 191–197. [CrossRef]
8. Kinoshita, Y.; Ichiryu, T.; Suzuki, A.; Ishida, H. 100 A Solid State Circuit Breaker Using Monolithic GaN Bidirectional Switch with Two-Step Gate-Discharging Technique. In Proceedings of the Institute of Electrical and Electronics Engineers, APEC 2020: Thirty-Fifth Annual IEEE Applied Power Electronics Conference and Exposition, New Orleans, LA, USA, 15–19 March 2020.
9. Li, H.; Li, X.; Wang, X.; Lyu, X.; Cai, H.; Alsmadi, Y.M.; Liu, L.; Bala, S.; Wang, J. Robustness of 650-V Enhancement-Mode GaN HEMTs under Various Short-Circuit Conditions. *IEEE Trans. Ind. Appl.* **2019**, *55*, 1807–1816. [CrossRef]
10. Suzuki, A.; Ichiryu, T.; Kinoshita, Y.; Ishida, H.; Handa, H.; Hatsuda, T. 300 A Solid State Circuit Breaker using Parallel Connected GaN Bidirectional Switch. In Proceedings of the Institute of Electrical and Electronics Engineers. PCIM Europe Digital Days 2020; International Exhibition and Conference for Power Electronics, Intelligent Motion, Renewable Energy and Energy Management, Nuremberg, Germany, 7–8 July 2020.
11. Askan, K.; Bartonek, M.; Stueckler, F. Bidirectional Switch Based on Silicon High Voltage Superjunction MOSFETs and TVS Diode Used in Low Voltage DC SSCB. In Proceedings of the Institute of Electrical and Electronics Engineers. PCIM Europe 2019; International Exhibition and Conference for Power Electronics, Intelligent Motion, Renewable Energy and Energy Management, Nuremberg, Germany, 7–9 May 2019.
12. Shen, Z.J.; Miao, Z.; Roshandeh, A.M.; Moens, P.; Devleeschouwer, H.; Salih, A.; Padmanabhan, B.; Jeon, W. First Experimental Demonstration of Solid State Circuit Breaker (SSCB) Using 650V GaN-based Monolithic Bidirectional Switch. In Proceedings of the IEEE Electron Devices Society and Institute of Electrical and Electronics Engineers, 2016 28th International Symposium on Power Semiconductor Devices and ICs (ISPSD), Prague, Czech Republic, 12–16 June 2016.
13. Adhikari, J.; Yang, T.; Rashed, M.; Bozhko, S.; Zhang, J.W.; Wheeler, P.W. Transient Stability Analysis of DC Solid State Power Controller (SSPC) for More Electric Aircraft. In *SAE Technical Papers*; SAE International: Warrendale, PA, USA, 2018. [CrossRef]
14. Molligoda, D.; Chatterjee, P.; Gajanayake, C.; Gupta, A.; Tseng, K.J. Review of design and challenges of DC SSPC in More Electric Aircraft. In Proceedings of the IEEE Power Electronics Society and Institute of Electrical and Electronics Engineers, 2016 IEEE 2nd Annual Southern Power Electronics Conference (SPEC), Auckland, New Zealand, 5–8 December 2016.
15. Rigogiannis, N.; Voglitsis, D.; Papanikolaou, N. Microcontroller Based Implementation of Peak Current Control Method in a Bidirectional Buck-Boost DC-DC Converter. In Proceedings of the 2018 20th International Symposium on Electrical Apparatus and Technologies (SIELA), Bourgas, Bulgaria, 3–6 June 2018; pp. 1–4. [CrossRef]